Front. Optoelectron.
DOI 10.1007/s12200-015-0502-2

RESEARCH ARTICLE

Water cooling radiator for solid state power supply in fast-axial-flow CO_2 laser

Heng ZHAO, Bo LI, Wenjin WANG, Yi HU, Youqin WANG (✉)

National Engineering Research Center for Laser Processing, School of Optical and Electronic Information, Huazhong University of Science and Technology, Wuhan 430074, China

Abstract Two different flow channel configurations on thermal resistances associated with the behavior of cooling of power device were studied in this paper. ANSYS Icepak 14.0 has been adopted as a numerical simulation tool. The simulation results from this study showed that the shapes of channels in cooling radiator play an important role in the thermal management of water cooling radiation system. The optimal channel design could improve the heat-dissipating efficiency by 80% in water cooling radiation system. The result also indicated that the thermal resistance of heat sinks decreased with the volumetric flow rate and the number of cylindrical columns in the flow channel. Experimental results were obtained under certain channel configurations and volume rates. Moreover, the results of numerical simulation can be explained well by the experimental results.

Keywords heat spreader, water cooling, turbulence generator, Icepak software

1 Introduction

The fast-axial-flow radio frequency (RF)-excited CO_2 laser is applied in current research areas like nano-particle synthesis, generation of mono-energetic million electron volts (MeV) photons in laser synchrotron sources, 13.5 nm extreme ultraviolet (EUV) sources for the next generation high volume chip manufacturing, particle acceleration, etc [1–4]. The performance of high-power fast-axial-flow RF-excited CO_2 laser is directly determined by the stable RF gas mixtures glow discharges in the discharge tube. The stable gas discharges is strongly influenced by the efficiency of solid state power supply. Power metal-oxide-semiconductor field-effect transistor (MOSFET) as one of core component of solid state power supply is usually operated under severe conditions of high power dissipation, consequently high junction temperatures may lead to poor reliability and ultimately premature failure of components [5]. As power density requirements grow for power converters, thermal management design for power devices has become an important factor [6]. Therefore, thermal management is a crucial step in the design of high efficiency solid state power supply. To find the most efficient way to control temperature and remove heat at power device for safe and reliable operation, a large number of researchers studied the thermal management of power device. Bar-Cohenand Iyengar [7] presented some useful research results on air-cooling heat sinks in power device cooling issues. In their studies, a number of fin designs and their manufacturing technologies, as well as performed optimization to identify the maximum heat transfer capability within a given design domain were considered. For the sake of studying the influence of more parameters on air-cooling heat sinks, Ozturk and Tari [8] analyzed three different commercial air-cooling heat sinks designed by using fluid dynamics software packages Icepak. The number of fins and their distribution, the fin material, and the base plate thickness were investigated in their study. Especially, replacing aluminum with copper as the heat sinks material improves the performance of whole system. However, the volume occupied and noise associated with the heat dissipation modules were always encountered in air-cooling heat sinks designs compared with liquid-cooling system. Advanced cooling techniques involving forced liquid convection, phase change and micro channel cooling system were drawn more attention to current and future semiconductor devices [9]. Lee [10] concentrated on a process of applying a computational fluid dynamics (CFD) technique to optimize pin array design of an integrated liquid-cooling insulated gate bipolar transistor (IGBT) power module. By simulating

Received December 15, 2014; accepted January 26, 2015

E-mail: yqwang13@163.com

different pin array designs, the effects of total convective area and fluid pattern on die temperature were examined. From Lee's studies, the two rows of rectangular pins along with the inclined deflecting plates were the best array design. Moores et al. [11] investigated heat dissipation effect of cooling fin heights design on an aluminum silicon carbide metal matrix composite base plate with integral cooling fins by using the thermal analysis and experimental performance. The studies showed 2 mm was the best height for cooling fin in this heat sink system. Nevertheless, the effect of the different shapes design of channel in liquid-cooling heat dissipating plate on heat dissipation has not been studied in Refs. [10,11]. At the system level, in order to radiate heats from power device more effectively, it is necessary to study the flow channel configurations. Thus, the purpose of this paper is to investigate the different shapes of channel and flow rates in water cooling radiation designs by using ANSYS Icepak 14.0 and to improve them based on the results of the analyses. In this paper, we took Mircosemi's MOSFET product DRF 1201 as the research objective, which is used as power device for 13.56 MHz solid state power supply in fast-axial-flow (FAF) laser. The investigations include numerical simulation and experimental verification. First, in order to obtain the better performance of heat radiation from the model power device on water cooling radiation, the geometric configurations of the flow channels were simulated with two designs (the S channel and the cylindrical channel). The nine different flow rates were also simulated by Icepak. We found that the cylindrical channel can improve heat dissipation effect and get lower peak temperature. Meanwhile, the thermal resistance of heat sinks decreases by increasing the volumetric flow rate and the number of cylindrical columns in the flow channel. Secondly, the water cooling radiation inlay different shapes of channel are manufactured by computer numerical control(CNC) machine tools. The nine different flow rates have been measured by flow meter. The surrounding temperature of power device on the water cooling radiation is monitored by Fluke Ti9 infrared thermal imager. Finally, the numerical simulation results can be explained well by the above experimental performance and the experimental result can verify the improved heat radiation performance.

2 Model building

In this study, the water cooling radiation system is shown in Fig. 1. Heat dissipation by the power MOSFET is derived from various flow channels embedded in the heat radiator. In this study, the power generated by the power MOSFET was simulated by heating block as shown in Fig. 2. The four heating blocks with different power level were used to simulate four different MOSFETs. The heat generated by heating block was transferred to the heat radiator through conduction heat transfer. The water which is flowing in heat radiator can take away heat. The loop of water-cooling was completed by pumps which keep the water temperature constant in inlet. Therefore, a typical water cooling radiation system consists of heat spreader, coolant, pump, water tank, and so on [12].

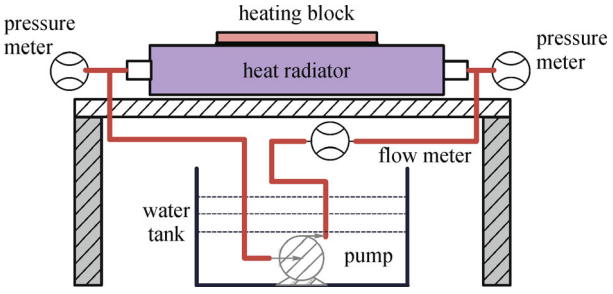

Fig. 1 Schematic diagram of water cooling radiation system

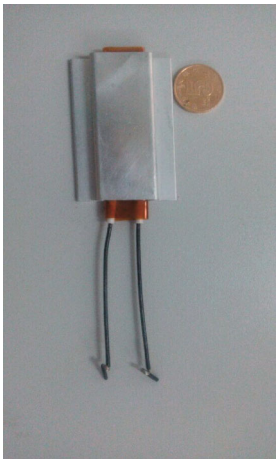

Fig. 2 Photographs of the heating block

To improve the effectiveness of heat radiation for the power MOSFET, two different flow channel designs for the water cooling radiator were used in this study, one is S flow channel design(see Fig. 3), the other is cylindrical columns flow channel design (see Fig. 4). Figure 5 is the photograph of the modules described above. The geometric configurations of water cooling radiator for the testing pieces were done by Solidworks 2012. HMC50 CNC machine tools were used to manufacture the testing pieces.

3 Governing equations

In this study, the basic assumptions for numerical simulation are described as follows: 1) Cooling pure water is incompressible normal properties fluid; 2) The relative velocity between a fluid and a solid is zero that means non-slip condition; 3) Only the forced convection effect is accounted for, the buoyancy effect is ignored;

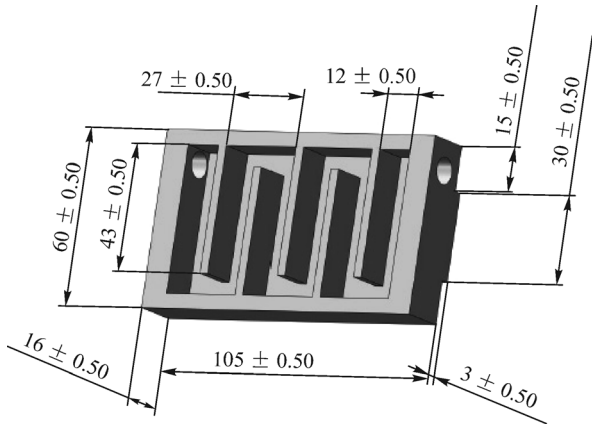

Fig. 3 Engineering drawing of heat spreader with S flow channel design, the unit dimension is mm

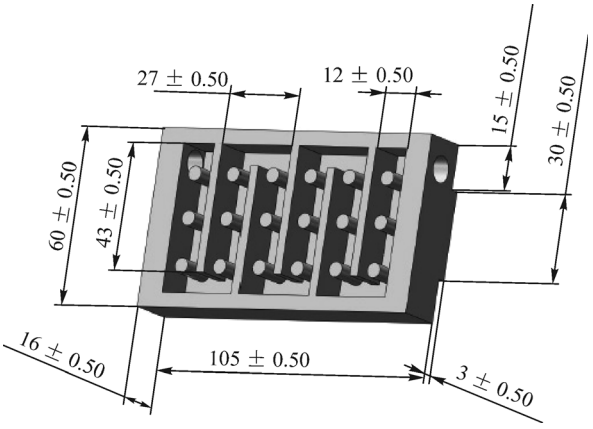

Fig. 4 Engineering drawing of heat spreader with cylindrical columns flow channel design, the unit dimension is mm

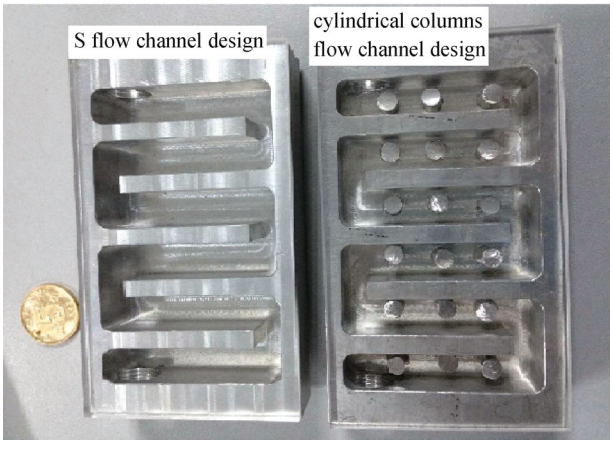

Fig. 5 Photograph of water-cooling heat spreader with different flow channel designs

4) The viscous dissipation is accounted for; 5) The regime of cooling pure water is steady-state.

Some nomenclatures were used in governing equations is listed in Table 1.

Table 1 Nomenclatures were used in governing equations

parameter	description	unit
Re	Reynolds number of channel	–
R_{th}	effective thermal resistance	–
E	total energy	J
u	velocity	$m \cdot s^{-1}$
k	turbulence kinetic energy	$m^2 \cdot s^{-2}$
p	pressure	Pa
h	heat transfer coefficient	$W \cdot m^{-2} \cdot k^{-1}$
H	channel height	m
Q	heat transfer capacity	W
T	temperature	K
ρ	density	$Kg \cdot m^{-3}$
λ	thermal conductivity	$W \cdot m^{-1} \cdot k^{-1}$
μ	fluid viscosity	$Kg \cdot m^{-1} \cdot s^{-1}$
ε	turbulent energy dissipation rate	$m^{2'} s^{-3}$
α	inverse effective Prandtl numbers	–
Δ	difference	–

The three dimensional thermal and flow fields is simulated by the commercial code fluent. Equations (1)–(3) represent the energy equation, the continuity equation and the momentum equations. The energy equation is employed to solve the temperature field. The governing equations for the fluid flow are the following continuity equation, momentum equations in three directions (x, y, and z), and energy equation. In this study, as the heat spreader with S flow channel design, the flow is observed as laminar. Due to the presence of the cylindrical columns in the improved circular flow channel designs, the flow with those channel designs is turbulent. Thus, renormalization group (RNG) k-ε turbulence model is used in this numerical simulation. The following closure Eqs. (4) and (5) [13] have been adopted to assess the turbulent viscosity and energy dissipation rate.

$$\frac{\partial}{\partial x_j}[u_i(\rho E + P)] = \frac{\partial}{\partial x_j}\left(\lambda_{\text{eff}}\frac{\partial T}{\partial x_i}\right), \tag{1}$$

$$\frac{\partial}{\partial x_i}(\rho u_i) = 0, \tag{2}$$

$$\frac{\partial(\rho u_i u_j)}{\partial x_j} = -\frac{\partial p}{\partial x_i} + \frac{\partial}{\partial x_j}\left(\mu\frac{\partial u_i}{\partial x_j} - \rho u_i u_j\right), \tag{3}$$

$$\frac{\partial(\rho k)}{\partial t}+\frac{\partial(\rho k u_i)}{\partial x_i}=\frac{\partial}{\partial x_j}\left[\alpha_k \mu_{\text{eff}}\frac{\partial k}{\partial x_j}\right]+G_k+\rho\varepsilon, \quad (4)$$

$$\frac{\partial(\rho\varepsilon)}{\partial t}+\frac{\partial(\rho\varepsilon u_i)}{\partial x_i}=\frac{\partial}{\partial x_j}\left[\alpha_\varepsilon \mu_{\text{eff}}\frac{\partial \varepsilon}{\partial x_j}\right]+G_k\frac{C_{1\varepsilon}^{*}\varepsilon}{k}-C_{2\varepsilon}\rho\frac{\varepsilon^2}{k}. \quad (5)$$

where G_k is the generation of turbulence kinetic energy due to the mean velocity gradients.

For the RNG k-ε turbulence model, the expressions or values of parameters in Eqs. (4) and (5) are summarized below:

$$C_{1\varepsilon}^{*}=C_{1\varepsilon}-\frac{\eta\left(1-\frac{\eta}{\eta_0}\right)}{1+\beta\eta^3}, \quad (6)$$

$$\eta=(2E_{ij}\cdot E_{ij})^{\frac{1}{2}}\frac{k}{\varepsilon}, \quad (7)$$

$$E_{ij}=\frac{1}{2}\left(\frac{\partial u_i}{\partial x_j}+\frac{\partial u_j}{\partial x_i}\right), \quad (8)$$

where the value of constants are $\eta_0=4.377$, $\beta=0.012$, $C_{1\varepsilon}=1.42$, $C_{2\varepsilon}=1.68$, $\alpha_k=\alpha_\varepsilon=1.39$.

To present the simulation results, the following parameters can be defined as

$$\text{Re}=\frac{\rho u_{\text{m}} H}{\mu}, \quad (9)$$

$$R_{\text{th}}=\frac{T_{\max}-T_{\text{in}}}{Q}, \quad (10)$$

where u_{m} is the mean velocity in the channel inlet, $T_{\max}$ is the contact temperature between the heat spreader and the heating block, and T_{in} is the coolant inlet temperature.

4 Calculation and analysis

The above system of governing equations was numerically solved using finite volume method. A finite volume method converted governing equations to algebraic equations using an "upwind" scheme [14]. The simple algorithm was used to enforce mass conservation and to solve the problem of velocity-pressure coupling to obtain the pressure field [15,16]. The convergence criteria used to control the numerical solution for momentum and energy equations were 10^{-4} and 10^{-7} respectively. The numerical simulations were finished after about 2000 steps iteration and converge.

This fluid mechanics model is three-dimension steady incompressible viscous flow. The fluid control equations described in Section 3 were involved in the numerical computation process. After the numerical simulation, the residual of each variable has been reduced to 0.001, in accordance with the criteria. Figures 6–9 present results obtained from experimental and numerical studies on the thermal resistances of two different heat spreader flow channel designs, various volumetric flow rates, and two different power levels. The experiment results became lower than the simulation results as the flow velocity increases. A possible explanation is that in the experiment condition, the heating block exchange heat not only with heat spreader but also with the surrounding air. The heat exchange efficiency in the experiment condition was lower compared with numerical simulation condition. Generally, the error between simulation result and experiment result was less than 20% [17]. This indicates that simulation results of this study are reasonable.

It was also found that the higher the flow velocity is, the smaller the thermal resistance is. As the flow rates are greater than 11 mL/s, the decreasing of the thermal resistance is unconspicuous. Therefore, it may be concluded the optimal coolant flow velocity is nearby 11 mL/s for the heat spreader. Moreover, Figs. 6– 9 indicate that the thermal resistance with the cylindrical columns flow channel design is smaller than that with the S flow channel design during the same power level. For the heat spreader with S flow channel design, the flow regime is observed as laminar, rather than turbulent, which was observed as the heat spreader with cylindrical columns channel design. In the same heat dissipation power, turbulence model can take more heat than laminar model. That means the cylindrical columns flow channel design has better heat dissipation effect.

The pressure drops for the two types of heat spreader under different flow rates are shown in Figs. 10 and 11. It

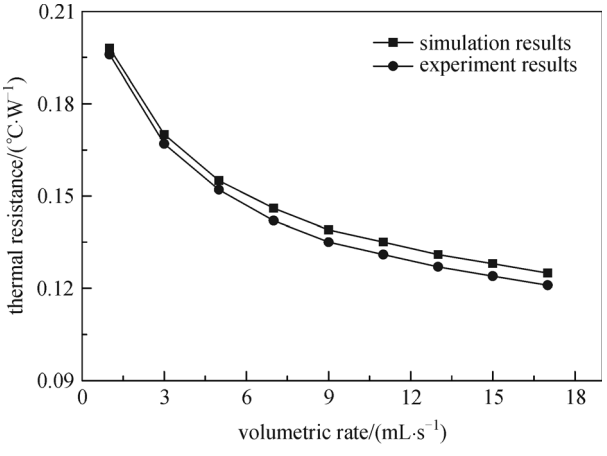

Fig. 6 Thermal resistances at various flow rates for heat spreader (@300 W) with S channel design

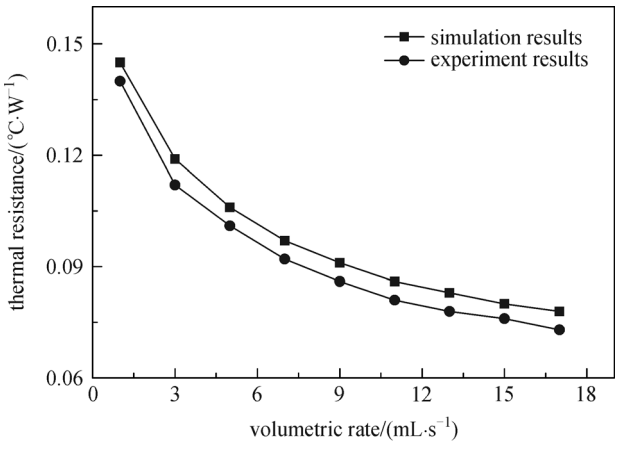

Fig. 7 Thermal resistances at various flow rates for heat spreader (@300 W) with cylindrical columns design

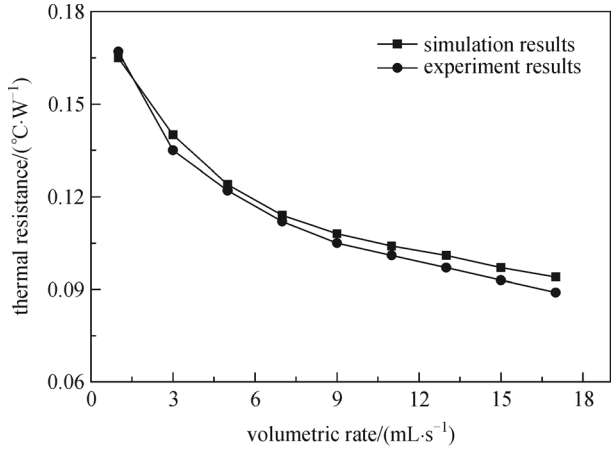

Fig. 8 Thermal resistances at various flow rates for heat spreader (@200 W) with S channel design

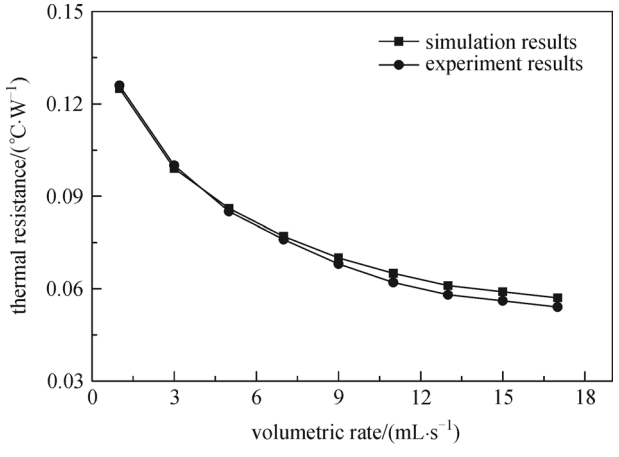

Fig. 9 Thermal resistances at various flow rates for heat spreader (@200 W) with cylindrical columns design

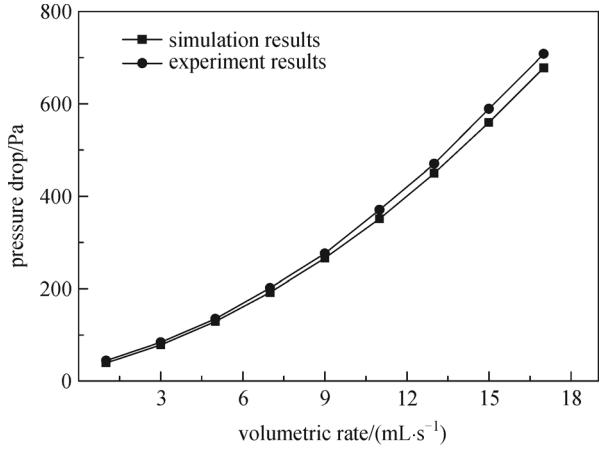

Fig. 10 Pressure drop at various flow rates for heat spreader (@300 W) with S channel design

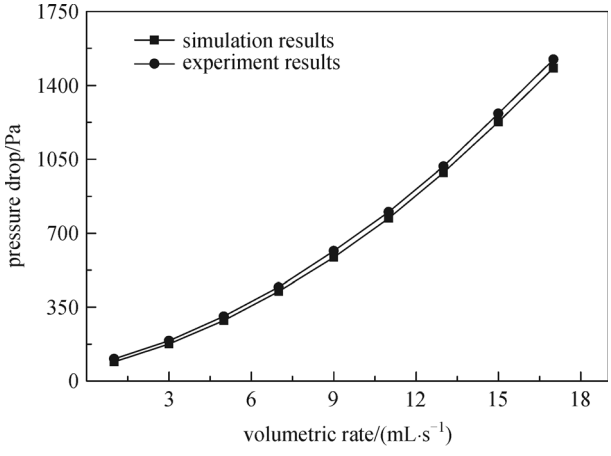

Fig. 11 Pressure drop at various flow rates for heat spreader (@300 W) with cylindrical columns design

can be seen that the pressure drop of cylindrical columns flow channel design was higher than that of S channel design under the condition of equal flow rates. The pressure drop is directly proportional to the pumping power required to move the cooling material through the heat sink [11]. The better dissipation effect was obtained by the cylindrical columns flow channel design. Meanwhile, the cylindrical columns flow channel design dissipated more pumping power than that of S channel design. For some engineering fields, such as heating, ventilation, air conditioning, and refrigeration systems, those designs are more sensitive to the changes of pumping power. However, for this study, the range of pressure drop is acceptable.

Figure 12 shows the contact temperature between the heat spreader and the heating block under different powers, which are generated by the heating block during coolant flow rate of 11 mL/s. Here, the environmental temperature

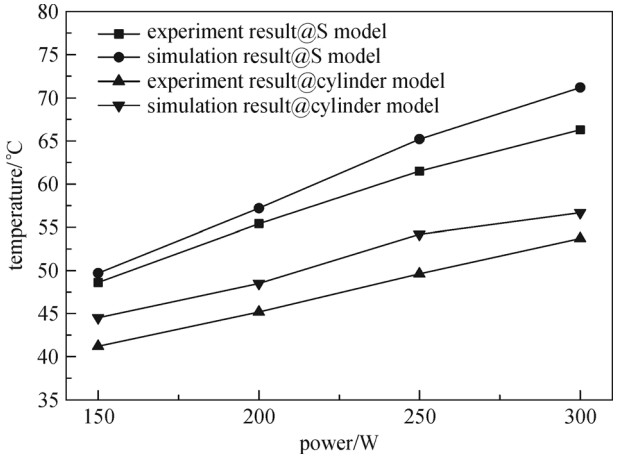

Fig. 12 Temperatures on the surface of heating block vs. pumping powers

is 25.2°C. From Fig. 12, we can see that the result of numerical simulation is slightly larger than experimental values. This is probably because the heating block does heat exchange with the surrounding air in the experimental condition, and the measurement error of measuring equipment also need to concern. Moreover, for the S channel design at power levels of 150 and 200 W, the temperature on the surface of heating block is lower than 82°C. The MOSFET can work normally. Here, the heating block was used to simulate MOSFET DRF1201. Because 82°C is considered as the high-temperature limit for the MOSFET [18]. However, for the S channel design at power level of 300 W, the temperature on the surface of heating block was 71.2°C. If the environmental temperature continues to rise, the MOSFET will be destroyed. Compared with the S channel design heat spreader, the cylindrical columns channel design heat spreader has better performance. The temperature on the surface of MOSFET was lower than 55°C at the power level of 300 W that means the cylindrical columns channel design heat spreader can adapt to more hostile environmental temperature.

5 Conclusions

This paper presents the heating performance of the heating powers of MOSFET based on different coolant flow rates and configuration of flow channels. Furthermore, numerical simulation and experimental validation were used to evaluate the heat dissipation capabilities of water cooling system. The following is a summary of the main results obtained in this investigation.

1) The heat transfer enhancement due to raising the coolant flow rates is more significant when the coolant flow rates are lower than 11 mL/s. In this study, the reduction of the thermal resistance was no more than 0.015°C/W when the flow rates were higher than 11 mL/s. Thus, the optimal coolant flow rate was 11 mL/s for the heat spreader system under this investigation.

2) Numerical simulation and experimental results showed that the flow channel design of heat spreader with turbulence flow leads to a reduction of thermal resistance more efficiently than the conventional S flow channel design with laminar flow.

3) The heat transfer enhancement of cylindrical columns channel design was considerable improvement compared with S flow channel design.

Acknowledgements This work was supported by the National Natural Science Foundation of China for Young Scholars (No. 61308045).

References

1. Sublemontier O, Lacour F, Leconte Y, Herlin-Boime N, Reynaud C. CO_2 laser-driven pyrolysis synthesis of silicon nanocrystals and applications. Journal of Alloys and Compounds, 2009, 483(1–2): 499–502
2. Kawashima Y. Proposal of a synchrotron radiation facility to supply ultraviolet light, X-ray, MeV-Photon, GeV-photon and neutron. In: Proceedings of FLS. 2006, WG112
3. Hoshino H, Suganuma T, Asayama T, Nowak K, Moriya M, Abe T, Endo A, Sumitani A. LPP EUV light source employing high-power CO2 laser. Proceedings on Advanced Lithography Technologies, 2008, 6921: 692131
4. Banna S, Berezovsky V, Schächter L. Particle acceleration by stimulated emission of radiation: theory and experiment. Physical Review E: Statistical, Nonlinear, and Soft Matter Physics, 2006, 74 (4 Pt 2): 046501–046514
5. Radivojevic Z, Andersson K, Bielen J A, van der Wel P J, Rantala J. Operating limits for RF power amplifiers at high junction temperatures. Microelectronics and Reliability, 2004, 44(6): 963–972
6. Van Wyk J D, Lee F C. Power electronics technology at the dawn of the new millennium-status and future. In: Proceedings of IEEE Power Electronics Specialists Conference. 1999, 1: 3–12
7. Bar-Cohen A, Iyengar M. Design and optimization of air-cooled heat sinks for sustainable development. IEEE Transactions on Components and Packaging Technologies, 2002, 25(4): 584–591
8. Ozturk E, Tari I. Forced air cooling of CPUs with heat sinks: a numerical study. IEEE Transactions on Components and Packaging Technologies, 2008, 31(3): 650–660
9. Zhang H, Liu J J, Li Y, Yao S C. Porous media modeling of two-phase micro-channel cooling of electronic chips with non-uniform power distribution. In: Proceedings of the American Society of Mechanical Engineers. 2013, 64481–64491
10. Lee T. Design optimization of an integrated liquid-cooled IGBT power module using CFD technique. IEEE Transactions on Components and Packaging Technologies, 2000, 23(1): 55–60
11. Moores K A, Joshi Y K, Schiroky G H. Thermal characterization of a liquid cooled AlSiC base plate with integral pin fins. IEEE Transactions on Components and Packaging Technologies, 2001, 24

(2): 213–219
12. Zhao D, Tan G. A review of thermoelectric cooling: Materials, modeling and applications. Applied Thermal Engineering, 2014, 66 (S1–2): 15–24
13. Yakhot V, Orszag S A. Renormalization group analysis of turbulence. I. Basic theory. Journal of Scientific Computing, 1986, 1(1): 3–51
14. Patankar S V. Numerical Heat Transfer and Fluid Flow. New York: Hemisphere Publishing Corporation, 1980, 36–78
15. Versteeg H K, Malasekera W. An Introduction to Computational Fluid Dynamics (The Finite Volume Method). London: Addison Wesley Longman Limited, 1995, 57–89
16. Hasan M I. Investigation of flow and heat transfer characteristics in micro pin fin heat sink with nanofluid. Applied Thermal Engineering, 2014, 63(2): 598–607
17. Yu X, Feng J, Feng Q, Wang Q. Development of a plate-pin fin heat sink and its performance comparisons with a plate fin heat sink. Applied Thermal Engineering, 2005, 25(2–3): 173–182
18. Microsemi. User Manual for DRF 1201 1, 2009

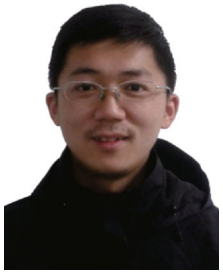

Heng Zhao is a Ph.D. candidate in the School of Optical and Electronic Information of Huazhong university of Science and Technology in Wuhan, Hubei, China. He received his B.S. degree in Huazhong University of Science and Technology. His current research interests include high power gas laser, integration of high power laser processing system and RF power amplifier.

Bo Li obtained his B.S., M.S. and Ph.D. degrees from Huazhong University of Science and Technology in 2000, 2003 and 2010. Currently, he is a lecturer of the School of Optical and Electronic Information of Huazhong University of Science and Technology. His research fields are high-power lasers and laser processing.

Wenjin Wang is a Ph.D. candidate, whose interests include research on a high-power CO_2 laser system design and optimization, gas discharge stability, and the kinetic modeling. Wang is with the School of Optical and Electronic Information, Huazhong University of Science and Technology, Wuhan, China.

Yi Hu is a Ph.D. candidate in the School of Optical and Electronic Information of Huazhong university of Science and Technology in Wuhan, Hubei, China. She received her B.S. degree in Huazhong University of Science and Technology.

Her current research interests include laser physics, laser optics, and high power laser industrial application.

Youqing Wang is a Professor and doctoral advisor, who has long been engaged in basic research on a high-power CO_2 laser and applied research on laser processing material. Wang is with the College of Optoelectronic Science and Technology, Huazhong University of Science and Technology, Wuhan, Hubei, China.